

---

# METRICS FOR EXPOSING THE BIASES OF CONTENT-STYLE DISENTANGLEMENT

**Xiao Liu\***, **Spyridon Thermos\***, **Gabriele Valvano\***, **Agisilaos Chartsias**  
 School of Engineering, University of Edinburgh, Edinburgh, UK  
 {Xiao.Liu, SThermos, G.Valvano, Agis.Chartsias}@ed.ac.uk

**Alison O’Neil<sup>1,2</sup>** & **Sotirios A. Tsafaris<sup>2,3</sup>**  
<sup>1</sup> Canon Medical Research Europe Ltd., Edinburgh, UK  
<sup>2</sup> School of Engineering, University of Edinburgh, Edinburgh, UK  
<sup>3</sup> The Alan Turing Institute, London, UK  
 Alison.ONeil@eu.medical.canon, S.Tsafaris@ed.ac.uk

## ABSTRACT

Recent state-of-the-art semi- and un-supervised solutions for challenging computer vision tasks have used the idea of encoding image content into a spatial tensor and image appearance or “style” into a vector. These decomposed representations take advantage of equivariant properties of network design and improve performance in equivariant tasks, such as image-to-image translation. Most of these methods use the term “disentangled” for their representations and employ model design, learning objectives, and data biases to achieve good model performance. While considerable effort has been made to measure disentanglement in vector representations, currently, metrics that can characterize the degree of disentanglement between content (spatial) and style (vector) representations and the relation to task performance are lacking. In this paper, we propose metrics to measure how (un)correlated, biased, and informative the content and style representations are. In particular, we first identify key design choices and learning constraints on three popular models that employ content-style disentanglement and derive ablated versions. Then, we use our metrics to ascertain the role of each bias. Our experiments reveal a “sweet-spot” between disentanglement, task performance and latent space interpretability. The proposed metrics enable the design of better models and the selection of models that achieve the desired performance and disentanglement. Our metrics library is available at [https://github.com/TsafarisCollaboratory/CSDisentanglement\\_Metrics\\_Library](https://github.com/TsafarisCollaboratory/CSDisentanglement_Metrics_Library).

## 1 INTRODUCTION

Recent work in representation learning argues that the good data representations should be able to separate out, or *disentangle*, the underlying explanatory factors into different dimensions of the considered latent space (Bengio et al., 2013; Higgins et al., 2018). In other words, it is beneficial to obtain representations that can separate latent variables that capture sensitive and useful information for the task at hand, from the ones that are less informative or even distracting. Over the years, disentanglement has been exploited to improve task performance, model generalization, and representation interpretability (Desjardins et al., 2012; Cohen & Welling, 2014; Reed et al., 2014; Yang et al., 2015; Kulkarni et al., 2015; Higgins et al., 2017; Siddharth et al., 2017; Patrick et al., 2018; Chartsias et al., 2019; Esser et al., 2019). However, the recent works of Locatello et al. (2019) and Locatello et al. (2020) indicate that unsupervised disentanglement is ill-posed and hence impossible, but that disentanglement can be achieved via biases imposed by model design, learning objectives, and data.

Inspired by these findings, we set out to expose several biases in state-of-the-art (SOTA) approaches to disentanglement. Our particular interest, and focus, is “content-style” disentanglement. Such

---

\*Authors contributed equally.

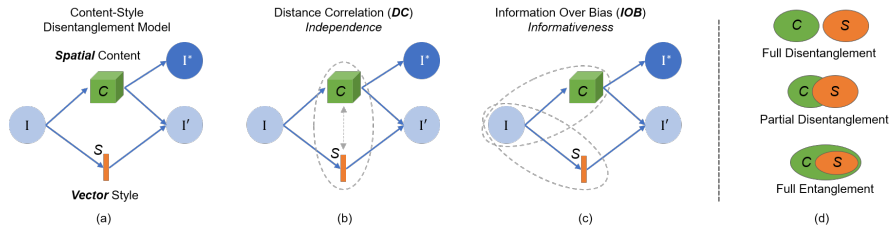


Figure 1: A schematic representation of disentanglement between spatial content  $C$  and vector style  $S$  (a) in the context of a main and a parallel spatially equivariant task ( $I'$ ,  $I^*$ ), followed by the proposed metrics that measure the distance correlation (b) between  $C$  and  $S$  (or between a latent variable and input  $I$ ), and the amount of information encoded in  $C$  or  $S$  with respect to the  $I$  bias (c). The rightmost part (d) is a visual dictionary of the different states of  $C$ - $S$  (dis)entanglement.

image decompositions into spatial “content” and vector “style” representations are employed to offer semi- or un-supervised solutions for challenging computer vision tasks. In principle, content variables should contain semantic information required for spatially equivariant tasks such as segmentation and pose estimation, whereas style variables contain residual information that controls aspects such as color intensity and texture. In practice, contrary to the extensive research efforts to quantify the intra-vector degree of disentanglement (Kumar et al., 2018; Chen et al., 2018; Eastwood & Williams, 2018; Ridgeway & Mozer, 2018; Karras et al., 2019; Xiao & Wang, 2019; Do & Tran, 2020), the separation between the content and style latent spaces is not typically assessed. In fact, to the best of our knowledge, there are no metrics to expose the relationship between the imposed biases and content-style disentanglement, and by extension the relationship of content-style disentanglement with model performance and latent space interpretability.

Our **contributions** (see also Fig. 1) are to:

- Introduce a set of complementary metrics to quantitatively evaluate content-style disentanglement in terms of: a) the amount of information encoded in each latent feature (informativeness); and b) the correlation between the encoded *spatial tensor* content and *vector* style features (independence).
- Identify key biases in three SOTA models that encourage content-style disentanglement, and expose how the biases affect disentanglement and task performance (utility). We focus on the popular vision tasks of image translation, segmentation, and pose estimation.
- Perform extensive experiments, where we find that lower disentanglement benefits task performance when the certain style-related priors are not violated, and that performance is correlated with latent variable informativeness. We also qualitatively assess the representation semanticness (interpretability).

## 2 RELATED WORK

**Content-style disentanglement:** Decoupling the style and content of an image has been extensively explored in Image-to-Image translation (I2I) (Liu et al., 2017; Lee et al., 2018; Huang et al., 2018). Outside I2I, content-style disentanglement has been used for many applications, such as semantic segmentation (Chartsias et al., 2019) and pose estimation (Charles et al., 2013), where the content has been used as a robust representation for a downstream task. In general, most methods use variants of (variational) auto-encoders to derive latent spaces that capture content/style information.

All of these models achieve content-style disentanglement using different biases, such as specific architectural choices (*e.g.* use of AdaIN (Huang & Belongie, 2017), content Binarization (Chartsias et al., 2019)), learning objectives (*e.g.* KL divergence and latent regression loss), or some supervision (*e.g.* using the content for a segmentation task (Chartsias et al., 2019)). However, the precise effect of each bias on the resulting disentanglement and model performance is not thoroughly explored.

**Current approaches for evaluating disentanglement:** The ideal approach for evaluating content-style disentanglement should: i) offer the ability to compare latent factors which are tensors of different dimensions (*e.g.* the style is a vector whereas the content is a spatial multi-channel tensor);

ii) be quantitative; and iii) not require ground truth information about the factors. Currently such approaches are lacking, but below we review related inspiring work.

A classical approach is *latent traversals*: a visualization that shows how traversing single latent dimensions generates variations in the image reconstruction. Latent traversals do not need ground truth information about the factors and can be used in mixed tensor spaces (e.g. as shown in Charsias et al. (2019) and Lorenz et al. (2019)), to offer qualitative evaluation. Alternatively, latent traversals can be combined with pretrained networks in order to measure the perceptual distance between produced embeddings (Karras et al., 2019). On the other hand, considerable effort exists in evaluating quantitatively the representations learned by VAEs and GANs, but all rely on vector representations and some also peruse ground truth knowledge of the latent factors. In particular, some methods try to associate known factors of variations (e.g. rotation and translation) with specific latent dimensions (Higgins et al., 2017; Kim & Mnih, 2018). Others measure the ability to isolate one factor in one individual vector latent variable (Kumar et al., 2018), measuring compactness or modularity (Chen et al., 2018; Eastwood & Williams, 2018; Xiao & Wang, 2019), linear separability (Karras et al., 2019), consistency and restrictiveness (Shu et al., 2020), and explicitness of the representation (Ridgeway & Mozer, 2018). On top of that, there are interesting works on measuring the informativeness of a specific factor of the vector latent variable w.r.t. the input, while also the independence among factors and their interpretability given some predefined concepts (Eastwood & Williams, 2018; Do & Tran, 2020).

**Impact:** The ability to transfer these concepts from the *vector*-based disentanglement (where they are defined) to the content-style disentanglement, which incorporates both spatial and vector representations, will expand our understanding of the relation between disentanglement and the: a) various biases adopted by each model; b) task performance; c) representation interpretability.

### 3 METRICS FOR CONTENT-STYLE DISENTANGLEMENT

Given  $N$  image samples  $\{I_i\}_{i=0}^N$ , we assume two representations of content and style features, defined as  $\{C_i\}_{i=0}^N$ , and  $\{S_i\}_{i=0}^N$ , respectively. We propose two metrics to evaluate properties that have been investigated in vector latent space disentanglement (Eastwood & Williams, 2018; Do & Tran, 2020): a) *independence*, and b) *informativeness*. Then, we discuss two properties of the representations, namely the *utility* and the *interpretability*, which will help us assess the advantages and disadvantages of content-style disentanglement.

#### 3.1 A MEASURE OF INDEPENDENCE: DISTANCE CORRELATION ( $DC$ )

Independent content and style variables satisfy  $p(C, S) = p(C)p(S)$ , but directly measuring independence with existing metrics is not feasible as these features generally are not probability distributions, and they have different dimensionality. We propose a proxy using the *Empirical Distance Correlation* ( $DC$ ) defined in Székely et al. (2007).  $DC$  measures the correlation between tensors of arbitrary dimensionality, and is bounded in the  $[0, 1]$  range. For  $N$  samples, consider two  $N$ -row matrices  $T_1$  and  $T_2$ . In general,  $T_1$  (or  $T_2$ ) have different column dimension as they are formed by concatenating images  $I_i$ , content features  $C_i$  or style features  $S_i$ . For  $I_i$  and  $C_i$  we first concatenate the channels and then row-scan to form a vector;  $S_i$  is already a vector.  $DC$  is then defined as:

$$DC(T_1, T_2) = \frac{dCov(T_1, T_2)}{\sqrt{dCov(T_1, T_1)dCov(T_2, T_2)}}, \quad (1)$$

while  $dCov$  is the distance covariance between any two  $N$ -row matrices  $X$  and  $Y$ , defined as:

$$dCov(X, Y) = \sqrt{\frac{1}{N^2} \sum_{i=1}^N \sum_{j=1}^N A_{i,j} B_{i,j}}, \quad (2)$$

where  $A$  and  $B$  correspond to distance matrices for  $X$  and  $Y$ , respectively. Note that each matrix element  $a_{i,j}$  of  $A$  is the Euclidean distance between two samples  $\|X^i - Y^j\|$ , after subtracting the mean of row  $i$  and column  $j$ , as well as the matrix mean.  $B$  is similarly calculated. Note that the contribution of Eq. 2 in measuring independence has already been investigated in the form of a de-correlation loss between two latent representations in Song et al. (2020). We estimate disentanglement between  $C$  and  $S$  by measuring their distance correlation,  $DC(C, S)$ , with lower values

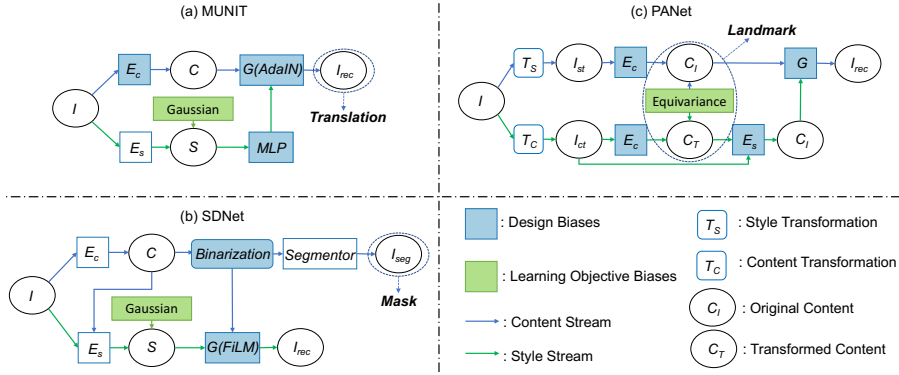


Figure 2: Model schematics. a) MUNIT:  $E_c$  uses Instance Normalization to remove style from content;  $E_s$  uses global pooling. b) SDNet: content is represented as binary images, and is used for segmentation. Style features minimize the KL divergence with a Gaussian distribution. c) PANet: training encourages content  $C$  and style  $S$  to be equivariant to spatial and intensity transformations.

(closer to 0) indicating higher disentanglement. Note that  $DC(C, S) = 0$  can also indicate full entanglement in the posterior collapse case, where all one latent variable encodes all the meaningful information and the other encodes only noise.

However, although  $DC(C, S)$  indicates the level of independence between  $C$  and  $S$ , it does not measure their informativeness: content and style can be uncorrelated while each containing only some portion of the image information, and more critically when one encodes *all* image information and the other *nothing*, *i.e.* noise. The latter has practical implications and is not uncommon (see Section 5): it largely originates due to posterior collapse when the decoder exclusively uses *e.g.* the content and ignores the other. To address this we introduce the next metric.

### 3.2 A MEASURE OF INFORMATIVENESS: INFORMATION OVER BIAS (IOB)

To explicitly measure the amount of information that  $C$  and  $S$  have, we propose the *Information Over Bias (IOB)* metric. Most importantly, *IOB* can detect the corner case, where  $C$  and  $S$  are disentangled because one is not informative about the input, *e.g.* posterior collapse. Given features  $z \in \{C, S\}$  produced from  $N$  image samples at inference, we aim to measure the amount of information encoded to each representation. That is, we train a decoder  $G_\theta$ , modeled as a neural network with parameters  $\theta$ , to reconstruct images  $I$ , given latent representations  $z$  predicted by the disentanglement framework. We argue that a post-hoc minimization of the Mean Square Error (MSE) between generated images  $\tilde{I}$  and ground truths  $I$  is equivalent to maximizing the log likelihood (based on the analysis in A.1). Thus, we define *IOB* as the ratio:

$$IOB(I, z) = \mathbb{E}_i \left[ \frac{\text{MSE}(I_i, G_\theta(\mathbb{1}))}{\text{MSE}(I_i, G_\theta(z_i))} \right] = \frac{\frac{1}{N} \sum_{i=1}^N \|I_i - G_\theta(\mathbb{1})\|^2 + \varepsilon}{\frac{1}{N} \sum_{i=1}^N \|I_i - \tilde{I}_i\|^2 + \varepsilon}, \quad (3)$$

where  $i = 1, \dots, N$  is the sample index and  $\varepsilon$  is a very small constant used to prevent division with zero. Notice that the ratio aims at ruling out from *IOB* both data biases (due to common structure, colors, pose, etc. across the images of the dataset) and architectural biases that one could introduce in the design of  $G_\theta$ . In particular, this is done by computing the ratio between MSE obtained after training  $G_\theta$  to reconstruct the images from their *informative* representation  $z$ , and after training  $G_\theta$  from an *uninformative* constant tensor  $\mathbb{1}$  (in this latter case,  $G_\theta$  will only learn the dataset bias it can model, given  $\theta$ ). As a result, high values of *IOB* can be associated with higher information inside the representation  $z$ , while the lower bound  $IOB = 1$  means that no information of the images  $I$  is encoded in  $z$ .<sup>1</sup> Since *IOB* requires the post-hoc training of  $G_\theta$  with gradient descent, we acknowledge the limitations of computation speed.

<sup>1</sup>The optimization process, *e.g.* stochastic gradient descent, can introduce noise in the final performance of the model. As a result, the actual value of *IOB* could be slightly smaller than 1 in practice.

---

### 3.3 UTILITY AND INTERPRETABILITY

To understand the effects of the level of  $C$ - $S$  disentanglement, measured quantitatively using  $DC$  and  $IOB$ , we investigate its relationship with the *utility* and *interpretability* of the learned representations. Utility refers to the performance on a downstream task, which for disentangled representations is typically image translation (Huang et al., 2018; Lee et al., 2018) to translate image content from one domain to another. We also consider tasks using content *e.g.* to extract segmentations (Chartsias et al., 2019) or landmarks (Lorenz et al., 2019), and therefore assess how effectively it can be used in downstream tasks. We detail this specifically for each application in Section A.2.

Assessing interpretability is far from trivial. Here, we assume that interpretability implies semantic representations. Previously, vector representations were considered semantic if a portion of the latent space corresponded to specific data variations (Chen et al., 2016). In disentangled representations, the style semantics were qualitatively evaluated with latent traversals of individual dimensions (Chartsias et al., 2019). Thus, we consider a style interpretable if images produced by linear traversals in the style latent space are realistic and smoothly change intensity. In spatial representations, such data variation should be confined to individual objects: thus, a semantic content should split objects in separate channels of  $C$ . We evaluate this with qualitative visuals wherever possible.

## 4 APPLICATIONS

Many applications disentangle content from style (Bouchacourt et al., 2018; Gabbay & Hoshen, 2020) or other attributes, such as pose, geometry, and motion (Denton & Birodkar, 2017; Villegas et al., 2017; Hsieh et al., 2018; Xing et al., 2019), to boost model performance in vision tasks. It is virtually impossible to analyse all of them, so we select and discuss three recent approaches from diverse applications in image translation (MUNIT (Huang et al., 2018)), semantic segmentation (SDNet (Chartsias et al., 2019)), and pose estimation (PANet (Lorenz et al., 2019)). All resemble auto-encoders, mapping input images to disentangled features, as shown in Fig. 2, but peruse several biases at various degrees.

We report a detailed model description and summarize *design* and *learning* biases in Section A.2, while here we describe how each bias is enforced. **a) MUNIT:** we consider ablations without Instance Normalization (IN) (Ulyanov et al., 2016), and AdaIN layers, as well as without style Latent Regression (LR).<sup>2</sup> Moreover, to assess the utility of the content  $C$ , we utilize  $C$  to complete a post-hoc task: we train a simple model using  $C$  as input to recognize objects that are presented in the data used to train the MUNIT model. **b) SDNet:** we identify content Binarization, Gaussian approximation, LR and the FiLM-based decoder as the main biases that affect content-style disentanglement and investigate their impact on the learned representations, as well as on the segmentation performance that is the main task of SDNet. **c) PANet:** we remove the Gaussian approximation and replace the specialized content-style conditioning with AdaIN. We also evaluate the importance of the equivariance loss with a hyperparameter sweep on different value ranges. Experiments are performed on pose estimation, the main task of PANet.

**Why these models?** We choose these models as they are well-known SOTA in the corresponding domains and cover the cases of: a) no supervision and weak  $C$  constraints (MUNIT), b) no supervision with strong  $C$  constraints (PANet), and c) supervision with strong  $C$  constraints (SDNet).

## 5 EXPERIMENTS

For each model, we analyze how design choices and learning objectives affect content-style disentanglement and the performance on respective tasks. We also evaluate the utility and interpretability of the learned representations. We use the model implementations provided by the authors, and the data they use to train and evaluate them, ablating only the specific components needed for our analysis. In all tables, arrows indicate the improvement direction of the metric and the best results are in bold. Numbers are the average of 5 different runs obtained with different weight initializations. Data description and detailed learning setup can be found in Sections A.3, A.4, and A.7.

---

<sup>2</sup>For fairness, we do not remove content LR as it is a fundamental part of the learning process of the model, and its absence severely affects performance.

Table 1: Comparative evaluation of MUNIT variants, using the proposed metrics. *FID* and *LPIPS* are used to assess translation quality and diversity between SYNTHIA (Ros et al., 2016) and Cityscapes (Cordts et al., 2016) samples. Results are presented in “mean  $\pm$ std” format.

MUNIT	Original Model	Design Bias		Learning Bias
		w/o AdaIN	w/o Instance Normalization (IN)	w/o Latent Regression (LR)
$DC(C, S)$ ( $\downarrow$ )	0.44 $\pm$ 0.06	0.43 $\pm$ 0.01	0.66 $\pm$ 0.03	<b>0.40</b> $\pm$ 0.08
$DC(I, C)$ ( $\uparrow$ )	0.57 $\pm$ 0.07	0.58 $\pm$ 0.08	<b>0.73</b> $\pm$ 0.03	0.57 $\pm$ 0.08
$DC(I, S)$ ( $\uparrow$ )	0.70 $\pm$ 0.02	0.56 $\pm$ 0.03	0.63 $\pm$ 0.05	<b>0.73</b> $\pm$ 0.03
$IOB(I, C)$ ( $\uparrow$ )	4.36 $\pm$ 0.38	4.85 $\pm$ 0.10	<b>5.01</b> $\pm$ 0.12	4.34 $\pm$ 0.58
$IOB(I, S)$ ( $\uparrow$ )	1.31 $\pm$ 0.04	1.17 $\pm$ 0.04	1.28 $\pm$ 0.06	<b>1.46</b> $\pm$ 0.05
<i>FID</i> ( $\downarrow$ )	73.48 $\pm$ 8.35	<b>52.48</b> $\pm$ 5.03	71.4 $\pm$ 4.86	104.51 $\pm$ 4.21
<i>LPIPS</i> ( $\uparrow$ )	0.08 $\pm$ 0.01	0.06 $\pm$ 0.01	<b>0.10</b> $\pm$ 0.01	0.09 $\pm$ 0.01

### 5.1 IMAGE-TO-IMAGE TRANSLATION: MUNIT ON SYNTHIA-CITYSCAPES

**Setup:** We consider the original MUNIT and three variants: **i)** we replace the AdaIN modules of the decoder with simple style concatenations, reducing the restrictions on the re-combination of  $C$  and  $S$  while decoding. **ii)** We remove the LR loss, which is responsible for the style Gaussianity. **iii)** We remove IN from the content encoder, to confirm that it helps the encoder to focus on the content only, and to discard the original style (Huang & Belongie, 2017). As Huang et al. (2018) we evaluate the quality and diversity of the translated images using the Fréchet Inception Distance (*FID*) (Heusel et al., 2017) and LPIPS (Zhang et al., 2018), respectively.

**Results:** Table 1 reports the results of the ablations on the SYNTHIA (Ros et al., 2016) and Cityscapes (Cordts et al., 2016) datasets. Replacing AdaIN (**w/o AdaIN**) with simple concatenation does not affect the level of  $C$ - $S$  disentanglement, but it leads to a 0.14 absolute decrease of  $IOB(I, S)$  and  $DC(I, S)$ , indicating that the style becomes less informative and less correlated with the input. Here, we observe an information shift to the content (lower  $IOB(I, S)$ , higher  $IOB(I, C)$ ) which leads to better translation quality, but also the worst diversity (0.06 *LPIPS*). We believe that this variant is worse than the original model, which has more balanced quality/diversity scores. By removing the LR learning bias (**w/o LR**), we observe that the style is significantly more correlated to the input image. In this setup, the style distribution is no longer Gaussian, however, a good approximation of the multivariate Gaussian would discourage representing discriminative information to achieve independence between the dimensions. As a result, the style has more degrees of freedom to encode non-relevant information, which contributes to higher  $IOB(I, S)$  and higher  $C$ - $S$  disentanglement. Overall, this experiment leads to a significant translation quality decrease, while contrary to the analysis in Huang et al. (2018), the diversity is not negatively affected. Finally, by removing IN (**w/o IN**) we expect a more entangled content that will also encode some style information. Our expectations are confirmed by the decrease of  $C$ - $S$  disentanglement ( $DC(C, S) = 0.66$ ), and a more informative content, which is also more correlated to the input image. Interestingly, relaxing the content constraints for a task that does not require a strictly semantic content (e.g. image segmentation), leads to the best quality/diversity balance. Note that we define the best balance as achieving the highest average ranking in *FID* and *LPIPS* (e.g. the “w/o IN” model variant is the 1<sup>st</sup> in *LPIPS* and 2<sup>nd</sup> in *FID*, thus the best overall model).

**Summary:** Our experiments show there is a trade-off between the translation quality/diversity and disentanglement, for the synthetic-to-real image-to-image translation task.<sup>3</sup> Our metrics indicate that a partially disentangled  $C$ - $S$  space coupled with a near-Gaussian style latent space leads to the best quality/diversity performance. For MUNIT this is achieved by removing the IN design bias.

### 5.2 MEDICAL SEGMENTATION: SDNET ON ACDC

**Setup:** In SDNet, content binarization and style Gaussianity, obtained via KL divergence and LR costs, are the most important constraints on the representation. We evaluate their implications on the performance, together with the decoder design implications, by: **i)** removing content thresholding (w/o Binarization), **ii)** removing style Gaussianity constraints (w/o KL divergence and LR), and **iv)**

<sup>3</sup>Note that the effect of  $C$ - $S$  disentanglement on the task performance also depends on the data bias. An indicative example is the “edges-to-shoes” where the translation is between zero-style and normal images.

Table 2: Comparative evaluation of SDNet variants on the ACDC (Bernard et al., 2018) dataset with 1.5% annotation masks, using the proposed metrics. *Dice Score* is used to assess semantic segmentation performance. Results are presented in “mean  $\pm$ std” format.

SDNet	Original Model	Design Bias		Learning Bias
		SPADE	w/o Binarization	w/o KL Divergence and Latent Regression (LR)
$DC(C, S)$ ( $\downarrow$ )	0.49 $\pm$ 0.02	0.52 $\pm$ 0.01	<b>0.44</b> $\pm$ 0.00	0.64 $\pm$ 0.03
$DC(I, C)$ ( $\uparrow$ )	0.94 $\pm$ 0.01	0.93 $\pm$ 0.01	<b>0.98</b> $\pm$ 0.02	0.94 $\pm$ 0.01
$DC(I, S)$ ( $\uparrow$ )	0.43 $\pm$ 0.02	0.45 $\pm$ 0.01	0.44 $\pm$ 0.01	<b>0.66</b> $\pm$ 0.00
$IOB(I, C)$ ( $\uparrow$ )	4.71 $\pm$ 0.26	5.09 $\pm$ 0.00	<b>5.89</b> $\pm$ 0.22	4.84 $\pm$ 0.23
$IOB(I, S)$ ( $\uparrow$ )	1.00 $\pm$ 0.01	1.00 $\pm$ 0.04	0.98 $\pm$ 0.04	1.00 $\pm$ 0.04
<i>Dice Score</i> ( $\uparrow$ )	0.62 $\pm$ 0.02	<b>0.75</b> $\pm$ 0.02	0.63 $\pm$ 0.04	0.61 $\pm$ 0.04

considering a new decoder, obtained replacing the FiLM style conditioning with *SPADE* (Park et al., 2019). *SPADE* is less restrictive, and allows the style to encode more image-related information than just intensity values, such as texture (see Section A.5). We also assess model performance using the Dice Score (Dice, 1945; Sørensen, 1948).

**Results:** Table 5 reports the ablation results on the ACDC (Bernard et al., 2018) dataset. We would like to highlight that when using all available annotations (fully supervised learning), all SDNet variants achieve similar accuracies (see Section A.6 for more details), suggesting that strong learning biases, like supervised segmentation costs, make disentanglement less important. Thus, we consider the semi-supervised training case with minimal supervision, using only the 1.5% of available labelled data. Broadly speaking, the style does not encode much information in any SDNet variant, probably because all medical images in ACDC consist of similar styles (data bias), and reconstructing using an average style is enough to have low  $IOB(I, S)$ . However,  $C$ - $S$  disentanglement is still important to have a good content representation. For example, it is evident that intermediate levels of disentanglement (**SPADE**) lead to the best segmentation performance. In this variant, the disentanglement decreases compared to the original model, as some style information is probably leaked to the content (higher  $DC(C, S)$  and  $IOB(I, C)$ ). On the other hand, removing  $C$  binarization (**w/o Binarization**) also leads to more informative content, although since the correlation between  $C$  and  $S$  decreases, we assume that the extra encoded information is noise and not part of style (this can be a posterior collapse case). Lastly, removing the Gaussian prior constraints from the style latent space (**w/o KL and LR**) makes the model the least disentangled (highest  $DC(I, S)$ ), as there is no information bottleneck in  $S$ , and the Dice score slightly decreases.

**Summary:** We report disentanglement to have minimum effect on task performance when training with strong learning signals (*i.e.* supervised costs). In the semi-supervised setting, higher partial (dis)entanglement leads to better performance, while the amount of information in  $C$  alone is not enough to achieve adequate segmentation performance.

### 5.3 POSE ESTIMATION: PANET ON DEEPFASHION

**Setup:** Together with the original PANet Lorenz et al. (2019) model, we consider four possible variants, relaxing design biases on both content and style, and learning biases. In detail: **i)** we experiment with a different conditioning mechanism to re-entangle style and content, that consists of the use of AdaIN, rather than simply multiplying each style vector with a separate content channel (introducing a bias on  $S$ , similar to MUNIT). **ii)** We consider the case where, instead of learning a different style for each channel of the content, we extract a global style vector, predicted by an MLP (relaxing the tight 1:1 correspondence between  $C$  and  $S$  channels). **iii)** We also consider the case where each content part is not approximated by Gaussian distributions. In this case we cannot use the original decoder to combine  $C$  and  $S$ , and thus we reintroduce the style using AdaIN. **iv)** Finally, we tested the effect of the equivariance constraint, by removing it from the cost function.

**Results:** Table 3 reports results of the ablations on the DeepFashion (Liu et al., 2016) dataset. We assess model performance using the *SIM* (Bylinskii et al., 2019) metric to measure the similarity between the predicted and ground truth landmarks visualized as heatmaps. Whilst the original model is the best to predict landmarks, it only has intermediate levels of disentanglement (see  $DC(C, S)$ ). Using an **AdaIN**-based decoder always improves disentanglement as it has a strong inductive bias on the re-entangled representation (see  $DC(C, S)$  for AdaIN, and **AdaIN w/o Gaussian**), but leads to

Table 3: Comparative evaluation of the different PANet model variants on the DeepFashion (Liu et al., 2016) dataset, using the proposed metrics. *SIM* is used to measure the performance in terms of pose estimation from landmarks. Results are presented in “mean  $\pm$ std” format.

PANet	Original Model	Design Bias			Learning Bias
		AdaIN	MLP	AdaIN w/o Gaussian	w/o Equivariance
$DC(C, S)$ ( $\downarrow$ )	0.65 $\pm$ 0.01	0.36 $\pm$ 0.02	0.69 $\pm$ 0.03	<b>0.25</b> $\pm$ 0.01	0.76 $\pm$ 0.08
$DC(I, C)$ ( $\uparrow$ )	0.59 $\pm$ 0.01	0.56 $\pm$ 0.01	0.58 $\pm$ 0.02	0.53 $\pm$ 0.01	<b>0.60</b> $\pm$ 0.02
$DC(I, S)$ ( $\uparrow$ )	<b>0.83</b> $\pm$ 0.01	0.81 $\pm$ 0.01	0.82 $\pm$ 0.03	0.38 $\pm$ 0.06	0.82 $\pm$ 0.01
$IOB(I, C)$ ( $\uparrow$ )	1.50 $\pm$ 0.08	1.52 $\pm$ 0.08	1.49 $\pm$ 0.06	<b>1.53</b> $\pm$ 0.06	1.50 $\pm$ 0.08
$IOB(I, S)$ ( $\uparrow$ )	1.09 $\pm$ 0.04	1.10 $\pm$ 0.15	<b>1.21</b> $\pm$ 0.09	1.12 $\pm$ 0.09	1.13 $\pm$ 0.06
<i>SIM</i> ( $\uparrow$ )	<b>0.71</b> $\pm$ 0.02	0.64 $\pm$ 0.01	0.68 $\pm$ 0.01	0.58 $\pm$ 0.00	0.47 $\pm$ 0.04

worse landmark detection, as the representation adapts too much to the strongly biased decoder, and the content loses transferability to other tasks, and interpretability (see also Fig. 3 and 8). Using an **MLP** to encode style relaxes the specific conditioning between  $C$  and  $S$  (*design bias*) and reduces disentanglement, *i.e.* high  $DC(C, S)$ , due to the information shift from  $C$  to  $S$  as indicated by the higher  $IOB(I, S)$ . Here, a moderate decrease of disentanglement shows slightly lower task performance. Lastly, the equivariance cost is the most important factor for disentanglement and removing it (**w/o Equivariance**) leads to the most entangled representation (high  $DC(C, S)$ ), and to landmark detection accuracy decrease.

**Summary:** Overall, higher partial entanglement leads to better landmark detection. Again, balance is the key to improve auxiliary tasks. In PANet, partial disentanglement is achieved by carefully balancing design biases used to extract the style with its reintroduction to the content while decoding. Relaxing such biases with AdaIN or MLP makes landmark detection worse.

#### 5.4 DISCUSSION

We now discuss the relationship between  $C$ - $S$  disentanglement and inductive biases, model performance, interpretability of the latent representations. We emphasize that the proposed metrics are uncorrelated from each other, as supported by the correlation matrix presented in Section A.8.

**Do biases affect  $C$ - $S$  disentanglement?** The results of Section 5 illustrate that learning and design biases critically affect disentanglement. However, no evaluation can specifically characterise the relative importance of each one, since this depends on the data and the task. In MUNIT, disentanglement is mainly encouraged by the content-related design and learning biases. In fact, IN is key to removing style information from the content, as well as the content LR bias that is vital for the successful training of the model. Disentanglement in SDNet is susceptible to both types of biases. Having a SPADE decoder or the removing of content thresholding leads to more entangled representations, while using a learning constraint that makes the style Gaussian restricts its informativeness and encourages disentanglement. Similarly, PANet disentanglement is affected both by the design choice of approximating content with Gaussian distributions, and also by the equivariance of  $C$  and  $S$  with respect to spatial or intensity transformations, respectively.

**Does  $C$ - $S$  disentanglement lead to better performance?** To some extent, yes. More specifically, we find a clear trade-off between  $C$ - $S$  disentanglement and downstream task performance. In particular, we observe that lower disentanglement that is based on relaxing the content constraints (*e.g.* removing IN), and not based on removing biases that enforce style priors, such as the Gaussian distribution and  $C$ - $S$  equivariance, leads to better performance. Exceptions to this conclusion are model variants whose level of  $C$ - $S$  disentanglement is affected by representations that tend to encode noise instead of meaningful information when removing certain constrains, *e.g.* the binarization bias in SDNet.

**How interpretable is content representation?** Interpretability is hard to quantify without metrics. Here, we analyze it qualitatively in Fig. 3 (see Section A.9 for more visualizations). We consider the content interpretable if distinct objects appear in different channels. Content interpretability varies considerably across models. In particular, while MUNIT content seems to encode some spatial representation of the input, this is spread across channels because it is not constrained by a specific bias. On the other hand, SDNet and PANet original models exhibit factorized content



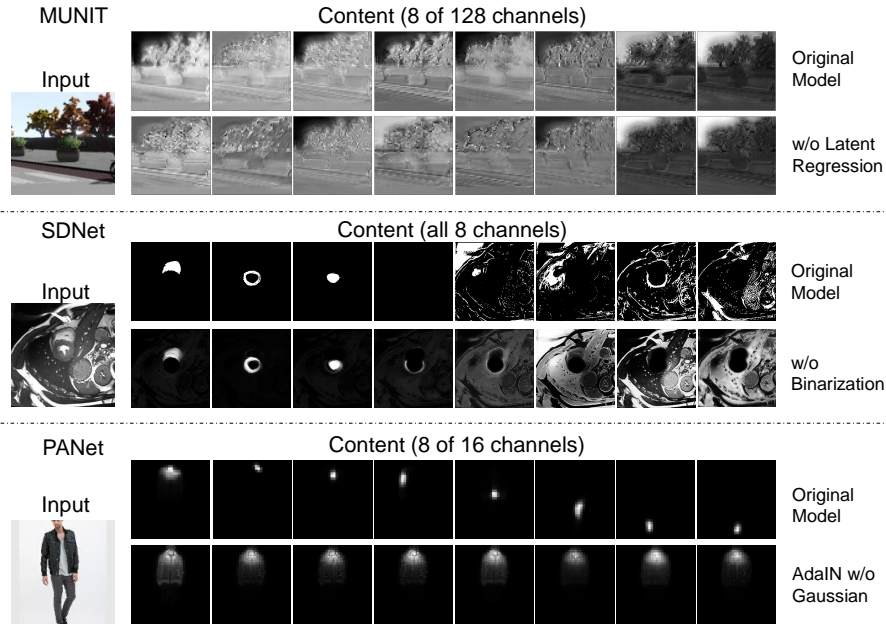


Figure 3: Content *interpretability* of each of the original models (top) and one of their variants (bottom). For each model, 8 channels of the content are visualized.

representations, with different objects, or parts, in different channels. In SDNet, a semantic content is encouraged by applying softmax and Binarization: this forces pixels to activate only in specific channels, and the model starts grouping together related structures. Analogous behaviour is obtained in PANet content, where the 2D Gaussian approximation of the body parts imposes an information bottleneck on every channel. To confirm this, we removed content constraints from SDNet and PANet, which results in spreading of spatial information across all channels, and in subsequent loss of interpretability.

## 6 CONCLUSION

We have proposed a set of metrics to evaluate the degree of disentanglement between image content and style. With these metrics, we performed extensive experiments on three state-of-the-art models to show how design and learning biases affect disentanglement. Such metrics are complementary to each other and, when used together, they can quantitatively assess the informativeness and the independence of the latent variables. Our findings suggest that content-style disentanglement is critically affected by the utilized biases, and that even though disentanglement enables the implementation of certain tasks, partially (dis)entangled representations can lead to better performance than fully disentangled ones. Additionally, our analysis suggests that strict constraints on the content representations lead to increased interpretability, which can be exploited in post-hoc tasks. Using the proposed metrics, future work will focus on designing training objectives to optimize for the sweet spot of disentanglement and performance, rather than pursuing very high (or low) disentanglement.

## REFERENCES

Alexander A Alemi, Ian Fischer, Joshua V Dillon, and Kevin Murphy. Deep variational information bottleneck. *arXiv preprint arXiv:1612.00410*, 2016.

Y. Bengio, A. Courville, and P. Vincent. Representation learning: A review and new perspectives. *IEEE Transactions on Pattern Analysis and Machine Intelligence*, 35(8):1798–1828, 2013.

Yoshua Bengio, Nicholas Léonard, and Aaron Courville. Estimating or propagating gradients through stochastic neurons for conditional computation. *arXiv preprint arXiv:1308.3432*, 2013.

- 
- Olivier Bernard, Alain Lalonde, and Clement Zotti *et al.* Deep learning techniques for automatic MRI cardiac multi-structures segmentation and diagnosis: is the problem solved? *IEEE Transactions on Medical Imaging (TMI)*, 37(11):2514–2525, 2018.
- Diane Bouchacourt, Ryota Tomioka, and Sebastian Nowozin. Multi-level variational autoencoder: Learning disentangled representations from grouped observations. In *Proc. AAAI Conference on Artificial Intelligence (AAAI)*, 2018.
- Zoya Bylinskii, Tilke Judd, Aude Oliva, Antonio Torralba, and Frédo Durand. What do different evaluation metrics tell us about saliency models? *IEEE Transactions on Pattern Analysis and Machine Intelligence (TPAMI)*, 41(3):740–757, 2019.
- James Charles, Tomas Pfister, Derek Magee, David Hogg, and Andrew Zisserman. Domain adaptation for upper body pose tracking in signed TV broadcasts. In *Proc. British Machine Vision Conference (BMVC)*, 2013.
- Agisilaos Chartsias, Thomas Joyce, Giorgos Papanastasiou, Scott Semple, Michelle Williams, David E. Newby, Rohan Dharmakumar, and Sotirios A. Tsaftaris. Disentangled representation learning in cardiac image analysis. *Medical Image Analysis*, 58, 2019.
- Ricky T. Q. Chen, Xuechen Li, Roger Grosse, and David Duvenaud. Isolating sources of disentanglement in VAEs. In *Proc. Advances in Neural Information Processing Systems (NeurIPS)*, pp. 2615–2625, 2018.
- Xi Chen, Yan Duan, Rein Houthoofd, John Schulman, Ilya Sutskever, and Pieter Abbeel. InfoGAN: Interpretable representation learning by information maximizing generative adversarial nets. In *Proc. Advances in Neural Information Processing Systems (NeurIPS)*, pp. 2172–2180, 2016.
- Taco S. Cohen and Max Welling. Learning the irreducible representations of commutative lie groups. In *Proc. International Conference on Machine Learning (ICML)*, pp. 1755–1763, 2014.
- Marius Cordts, Mohamed Omran, Sebastian Ramos, Timo Rehfeld, Markus Enzweiler, Rodrigo Benenson, Uwe Franke, Stefan Roth, and Bernt Schiele. The Cityscapes dataset for semantic urban scene understanding. In *Proc. IEEE Conference on Computer Vision and Pattern Recognition (CVPR)*, pp. 3213–3223, 2016.
- Emily Denton and Vighnesh Birodkar. Unsupervised learning of disentangled representations from video. In *Proc. Advances in Neural Information Processing Systems (NeurIPS)*, pp. 4414–4423, 2017.
- Guillaume Desjardins, Aaron Courville, and Yoshua Bengio. Disentangling factors of variation via generative entangling. In *arXiv preprint arXiv:1210.5474*, 2012.
- Lee R Dice. Measures of the amount of ecologic association between species. *Ecology*, 26(3): 297–302, 1945.
- Kien Do and Truyen Tran. Theory and evaluation metrics for learning disentangled representations. In *International Conference on Learning Representations (ICLR)*, 2020.
- Cian Eastwood and Christopher K. I. Williams. A framework for the quantitative evaluation of disentangled representations. In *International Conference on Learning Representations (ICLR)*, 2018.
- Patrick Esser, Johannes Haux, and Bjorn Ommer. Unsupervised robust disentangling of latent characteristics for image synthesis. In *Proc. IEEE International Conference on Computer Vision (ICCV)*, pp. 2699–2709, 2019.
- Aviv Gabbay and Yedid Hoshen. Demystifying inter-class disentanglement. In *International Conference on Learning Representations (ICLR)*, 2020.
- Martin Heusel, Hubert Ramsauer, Thomas Unterthiner, Bernhard Nessler, and Sepp Hochreiter. GANs trained by a two time-scale update rule converge to a local Nash equilibrium. In *Proc. Advances in Neural Information Processing Systems (NeurIPS)*, pp. 6626–6637, 2017.

- 
- Irina Higgins, Loic Matthey, Arka Pal, Christopher Burgess, Xavier Glorot, Matthew Botvinick, Shakir Mohamed, and Alexander Lerchner.  $\beta$ -VAE: Learning basic visual concepts with a constrained variational framework. In *International Conference on Learning Representations (ICLR)*, 2017.
- Irina Higgins, David Amos, David Pfau, Sebastien Racaniere, Loic Matthey, Danilo Rezende, and Alexander Lerchner. Towards a definition of disentangled representations. *arXiv preprint arXiv:1812.02230*, 2018.
- Jun-Ting Hsieh, Bingbin Liu, De-An Huang, Li F Fei-Fei, and Juan Carlos Niebles. Learning to decompose and disentangle representations for video prediction. In *Proc. Advances in Neural Information Processing Systems (NeurIPS)*, pp. 517–526, 2018.
- Xun Huang and Serge Belongie. Arbitrary style transfer in real-time with adaptive instance normalization. In *Proc. IEEE International Conference on Computer Vision (ICCV)*, pp. 1501–1510, 2017.
- Xun Huang, Ming-Yu Liu, Serge Belongie, and Jan Kautz. Multimodal unsupervised image-to-image translation. In *Proc. European Conference on Computer Vision (ECCV)*, pp. 179–196, 2018.
- Tero Karras, Samuli Laine, and Timo Aila. A style-based generator architecture for generative adversarial networks. In *Proc. IEEE Conference on Computer Vision and Pattern Recognition (CVPR)*, pp. 4401–4410, 2019.
- Hyunjik Kim and Andriy Mnih. Disentangling by factorising. In *Proc. International Conference on Machine Learning (ICML)*, pp. 2649–2658, 2018.
- Diederik P Kingma and Max Welling. Auto-encoding variational Bayes. *arXiv preprint arXiv:1312.6114*, 2013.
- Tejas D. Kulkarni, William F. Whitney, Pushmeet Kohli, and Josh Tenenbaum. Deep convolutional inverse graphics network. In *Proc. Advances in Neural Information Processing Systems (NeurIPS)*, pp. 2539–2547, 2015.
- Abhishek Kumar, Prasanna Sattigeri, and Avinash Balakrishnan. Variational inference of disentangled latent concepts from unlabeled observations. In *International Conference on Learning Representations (ICLR)*, 2018.
- Hsin-Ying Lee, Hung-Yu Tseng, Jia-Bin Huang, Maneesh Singh, and Ming-Hsuan Yang. Diverse image-to-image translation via disentangled representations. In *Proc. European Conference on Computer Vision (ECCV)*, pp. 36–52, 2018.
- Ming-Yu Liu, Thomas Breuel, and Jan Kautz. Unsupervised image-to-image translation networks. In *Proc. Advances in Neural Information Processing Systems (NeurIPS)*, pp. 700–708, 2017.
- Ziwei Liu, Ping Luo, Shi Qiu, Xiaogang Wang, and Xiaoou Tang. DeepFashion: Powering robust clothes recognition and retrieval with rich annotations. In *Proceedings of IEEE Conference on Computer Vision and Pattern Recognition (CVPR)*, pp. 1096–1104, 2016.
- Francesco Locatello, Stefan Bauer, Mario Lucic, Gunnar Rätsch, Sylvain Gelly, Bernhard Schölkopf, and Olivier Bachem. Challenging common assumptions in the unsupervised learning of disentangled representations. In *International Conference on Learning Representations Workshops (ICLRW)*, 2019.
- Francesco Locatello, Stefan Bauer, Mario Lucic, Gunnar Rätsch, Sylvain Gelly, Bernhard Schölkopf, and Olivier Bachem. A commentary on the unsupervised learning of disentangled representations. In *Proc. AAAI Conference on Artificial Intelligence (AAAI)*, pp. 13681–13684, 2020.
- Dominik Lorenz, Leonard Bereska, Timo Milbich, and Bjorn Ommer. Unsupervised part-based disentangling of object shape and appearance. In *Proceedings of the IEEE Conference on Computer Vision and Pattern Recognition*, pp. 10955–10964, 2019.

- 
- Taesung Park, Ming-Yu Liu, Ting-Chun Wang, and Jun-Yan Zhu. Semantic image synthesis with spatially-adaptive normalization. In *Proc. IEEE Conference on Computer Vision and Pattern Recognition (CVPR)*, pp. 2337–2346, 2019.
- Esser Patrick, Ekaterina Sutter, and Björn Ommer. A variational U-Net for conditional appearance and shape generation. In *Proc. IEEE Conference on Computer Vision and Pattern Recognition (CVPR)*, pp. 8857–8866, 2018.
- Ethan Perez, Florian Strub, Harm de Vries, Vincent Dumoulin, and Aaron C. Courville. FiLM: Visual reasoning with a general conditioning layer. In *Proc. AAAI Conference on Artificial Intelligence (AAAI)*, 2018.
- Scott Reed, Kihyuk Sohn, Yuting Zhang, and Honglak Lee. Learning to disentangle factors of variation with manifold interaction. In *Proc. International Conference on Machine Learning (ICML)*, pp. 1431–1439, 2014.
- Karl Ridgeway and Michael C. Mozer. Learning deep disentangled embeddings with the F-statistic loss. In *Proc. Advances in Neural Information Processing Systems (NeurIPS)*, pp. 185194, 2018.
- German Ros, Laura Sellart, Joanna Materzynska, David Vazquez, and Antonio M. Lopez. The synthia dataset: A large collection of synthetic images for semantic segmentation of urban scenes. In *Proc. IEEE Conference on Computer Vision and Pattern Recognition (CVPR)*, pp. 3234–3243, 2016.
- Rui Shu, Yining Chen, Abhishek Kumar, Stefano Ermon, and Ben Poole. Weakly supervised disentanglement with guarantees. In *International Conference on Learning Representations (ICLR)*, 2020.
- N. Siddharth, B. Paige, J.-W. van de Meent, A. Desmaison, N. D. Goodman, P. Kohli, F. Wood, and P. Torr. Learning disentangled representations with semi-supervised deep generative models. In *Proc. Advances in Neural Information Processing Systems (NeurIPS)*, 2017.
- Zengjie Song, Oluwasanmi Koyejo, and Jiangshe Zhang. Toward a controllable disentanglement network. *arXiv preprint arXiv:2001.08572*, 2020.
- Thorvald Sørensen. A method of establishing groups of equal amplitude in plant sociology based on similarity of species content and its application to analyses of the vegetation on danish commons. *Royal Danish Academy of Sciences and Letters*, 5(4):1–34, 1948.
- Gábor J Székely, Maria L Rizzo, Nail K Bakirov, et al. Measuring and testing dependence by correlation of distances. *The annals of statistics*, 35(6):2769–2794, 2007.
- Dmitry Ulyanov, Andrea Vedaldi, and Victor Lempitsky. Instance normalization: The missing ingredient for fast stylization. *arXiv preprint arXiv:1607.08022*, 2016.
- Ruben Villegas, Jimei Yang, Seunghoon Hong, Xunyu Lin, and Honglak Lee. Decomposing motion and content for natural video sequence prediction. In *International Conference on Learning Representations (ICLR)*, 2017.
- Yijun Xiao and William Yang Wang. Disentangled representation learning with Wasserstein total correlation. *arXiv preprint arXiv:1912.12818*, 2019.
- Xianglei Xing, Tian Han, Ruiqi Gao, Song-Chun Zhu, and Ying Nian Wu. Unsupervised disentangling of appearance and geometry by deformable generator network. In *Proc. IEEE Conference on Computer Vision and Pattern Recognition (CVPR)*, pp. 10354–10363, 2019.
- Jimei Yang, Scott E. Reed, Ming-Hsuan Yang, and Honglak Lee. Weakly-supervised disentangling with recurrent transformations for 3D view synthesis. In *Proc. Advances in Neural Information Processing Systems (NeurIPS)*, pp. 1099–1107, 2015.
- Richard Zhang, Phillip Isola, Alexei A. Efros, Eli Shechtman, and Oliver Wang. The unreasonable effectiveness of deep features as a perceptual metric. In *Proc. IEEE Conference on Computer Vision and Pattern Recognition (CVPR)*, pp. 586–595, 2018.

---

Jun-Yan Zhu, Richard Zhang, Deepak Pathak, Trevor Darrell, Alexei A Efros, Oliver Wang, and Eli Shechtman. Toward multimodal image-to-image translation. In *Proc. Advances in Neural Information Processing Systems (NeurIPS)*, pp. 465–476, 2017.

---

## A APPENDIX

### A.1 MAXIMIZING LIKELIHOOD BY MINIMIZING MEAN SQUARE ERROR

Let  $y$  denote a generic pixel in an image  $I$ , and  $\tilde{y}$  the respective pixel in the reconstructed image  $\tilde{I}$ , obtained through a learned decoding function.

If we assume the reconstruction error, denoted as  $\varepsilon$ , to be normally distributed (*i.e.*  $\varepsilon \sim \mathcal{N}(0, \sigma^2)$ ), then, the predicted value  $\tilde{y}$  is normally distributed around the true value  $y$ , thus  $\tilde{y} \sim \mathcal{N}(y, \sigma^2)$ . Based on this assumption, the probability density function can be defined as:

$$f(\tilde{y}|y, \sigma^2) = \frac{1}{\sqrt{2\pi\sigma^2}} e^{-\frac{(\tilde{y}-y)^2}{2\sigma^2}}. \quad (4)$$

Given a set of observations, *e.g.* the pixels of the image, we maximize the likelihood  $\mathcal{L}$  as the product of the probability densities of the observations:

$$\mathcal{L} = \prod_{i=1}^n f(y_i|\tilde{y}_i, \sigma^2) = (2\pi\sigma^2)^{-n/2} e^{-\frac{\sum_{i=1}^n (y_i - \tilde{y}_i)^2}{2\sigma^2}}. \quad (5)$$

Assuming the variance of the error to be independent from the input variables, optimizing the latter formula is equivalent to optimize:

$$\log\left(\frac{\mathcal{L}}{(2\pi\sigma^2)^{-n/2}}\right) = -\frac{\sum_{i=1}^n (y_i - \tilde{y}_i)^2}{2\sigma^2}. \quad (6)$$

Thus, maximizing the original likelihood function is equivalent to minimizing  $\sum_{i=1}^n (y_i - \tilde{y}_i)^2$ , that is the scaled Mean Squared Error (MSE). As a result, by training the decoder to minimize MSE, we train it to maximize the Mutual Information (MI) between  $z$  and  $I$ .

After training the decoder  $G_\theta$  (see Section 3, computing MSE equivalent to directly measuring the MI. There is a relationship between likelihood and MSE (shown below), but the likelihood acts as a lower bound to MI.

**Relationship MSE - likelihood:** Note that if we divide both parts of the equation by  $n$  and then we multiply by  $-2\sigma^2$ , we obtain:

$$\sum_{i=1}^n \frac{(y_i - \tilde{y}_i)^2}{n} = -\frac{2\sigma^2}{n} \cdot \log\left(\frac{\mathcal{L}}{(2\pi\sigma^2)^{-n/2}}\right), \quad (7)$$

that is:

$$MSE = -\frac{2\sigma^2}{n} \log(\mathcal{L}) - \sigma^2 \log(2\pi\sigma^2). \quad (8)$$

Since we assume homoscedastic distributions, *i.e.* fixed  $\sigma^2$ , Equation 8 can be expressed as:

$$MSE = -\frac{a}{n} \log(\mathcal{L}) - b, \quad (9)$$

where  $a$  and  $b$  are positive constants.

### A.2 DETAILED MODEL DESCRIPTION

**MUNIT for Image-to-Image Translation:** Multimodal Unsupervised Image-to-image Translation (MUNIT) (Huang et al., 2018) does not impose strict constraints on the learned representations, and achieves disentanglement with both design and learning biases. The basic assumption is that multi-domain images (a necessary *data bias*), share common content information, but differ in style. A content encoder maps images to multi-channel feature maps, by removing style with IN layers Huang & Belongie (2017) (*design bias*). A second encoder extracts global style information with fully connected layers and global pooling. Finally, style and content are combined in a decoder

Table 4: Overview of the *design* and *learning biases* that are investigated in the context of the three investigated vision tasks: a) image-to-image translation (MUNIT), b) medical segmentation (SDNet), and c) pose estimation (PANet).

		MUNIT	SDNet	PANet
<b>Design Bias</b>	AdaIN	✓		✓
	Instance Normalization	✓		
	SPADE		✓	
	Binarization		✓	
	MLP			✓
<b>Learning Bias</b>	Latent Regression	✓	✓	
	KL Divergence		✓	
	Equivariance			✓

with AdaIN modules Huang & Belongie (2017) (*design bias*). Disentanglement is additionally promoted with a bidirectional reconstruction loss Zhu et al. (2017) that enables style transfer. In order to learn a smooth representation manifold, two LR losses (*learning bias*) are applied on content and style extracted from input images: content LR penalizes the distance to the content extracted from reconstructed images, whereas style LR encourages encoded style distributions to match their Gaussian priors. Finally, adversarial learning encourages realistic synthetic images.

**SDNet for Medical Image Segmentation:** SDNet (Chartsias et al., 2019) is a semi-supervised framework that disentangles medical images in anatomical features (content) and imaging-specific characteristics (style). Similarly to other models, SDNet uses separate content and style encoders, but here a segmentation network is applied on the content features trained with supervised objectives and annotated images (*data bias*). However, in contrast to MUNIT, SDNet does not impose a design bias on the encoder, but rather on the content which is represented as multi-channel binary maps of the same resolution as the input (*design bias*). This is obtained with a softmax and a thresholding function with the straight-through operator Bengio et al. (2013), such that any style is removed from the content. To encourage style features to encode residual information (and not content), a loss enforces the style representation to approximate a standard Gaussian, following the VAE formulation Kingma & Welling (2013) (*learning bias*). In this setup, any information encoded in style comes at a cost, and thus encoding redundant information is prevented Alemi et al. (2016). Furthermore, a LR loss of the style is employed to prevent posterior collapse of the decoder (*learning bias*). Finally, style and content are combined to reconstruct the input image by applying a series of convolutional layers with feature-wise linear modulation (FiLM) conditioning Perez et al. (2018). Similarly to AdaIN, FiLM modules are restrictive, allowing the style only to normalize the conditioned feature maps, and thus further discouraging the style from encoding content information (*design bias*).

**PANet for Pose Estimation:** We finally consider a dual-stream autoencoder denoted as PANet (Lorenz et al., 2019), which is used for pose estimation. PANet consists of two branches that decouple pose (content) and appearance (style) but employs heavily entangled encoders-decoders. The content is represented as a multi-channel feature map, where each channel corresponds to a specific body part (since the number of parts are fixed, this imposes a strong *data bias*). A Gaussian distribution is applied to each feature map to remove any appearance (style) information, whilst also preserving the spatial correspondence (*design bias*). The corresponding style information is extracted from the encoder features using average pooling (*design bias*). More critically, style vectors do not correspond to global image style, since they are applied to specific content parts during decoding (*design bias*). Finally, disentanglement is encouraged with a transformation equivariance loss (*learning bias*). This ensures that the spatial transformations, such as translations and rotations, affect only the content, while the intensity ones, such as the color and texture information, affect only the style.

Table 4 summarizes the *design* and *learning biases* of the aforementioned methods. Note that the biases are reported as modules, without indicating the way they are used in the experiments (*e.g.* AdaIN is reported without specifying that it is removed from the original MUNIT, but is added to PANet as a variant).

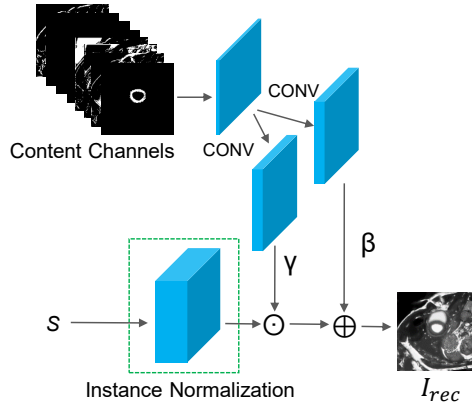


Figure 4: Detailed representation of the SPADE decoder (Park et al., 2019) in the context of SD-NET (Chartsias et al., 2019). Style is denoted as  $S$ , while CONV represents the convolution operation. Note that  $\gamma$  and  $\beta$  parameters are applied to the normalized style activations through element-wise multiplication and addition, respectively.

### A.3 SYNTHIA-CITYSCAPES DESCRIPTION AND MUNIT TRAINING SETUP

**Data:** We use SYNTHIA Ros et al. (2016), which consists of over 20,000 rendered images and corresponding pixel-level semantic annotations, where 13 classes of objects are labeled for aiding segmentation and scene understanding problems. We also use Cityscapes Cordts et al. (2016), which contains a set of diverse street scene stereo video sequences and over 5,000 frames of high-quality semantic annotations, where 30 classes of instances are labeled in the segmentation masks.

**Training setup:** MUNIT achieves unsupervised multi-modal image-to-image translation by minimizing the following loss function:

$$\mathcal{L}_{total} = \mathcal{L}_{GAN} + \lambda_1 \mathcal{L}_{rec} + \lambda_2 \mathcal{L}_{c-rec} + \lambda_3 \mathcal{L}_{s-rec}, \quad (10)$$

where  $\mathcal{L}_{rec}$  is the image reconstruction loss,  $\mathcal{L}_{c-rec}$  and  $\mathcal{L}_{s-rec}$  denote the content and style reconstruction losses, and  $\lambda_1 = 10$ ,  $\lambda_2 = 1$  are the hyperparameters used by the authors in Huang et al. (2018).

### A.4 ACDC DESCRIPTION AND SDNET TRAINING SETUP

**Data:** We use data from the Automatic Cardiac Diagnosis Challenge (ACDC) (Bernard et al., 2018), which contains cardiac cine-MR images acquired from different MR scanners and resolution on 100 patients. Images were resampled to  $1.37 \text{ mm}^2/\text{pixel}$  resolution and cropped to  $224 \times 224$  pixels. Manual segmentations are provided for the left ventricular cavity, the myocardium and right ventricle in the end-systolic and end-diastolic cardiac phases. In total there are 1920 images with manual segmentations and 23,530 images with no segmentations.

**Training setup:** SDNet is trained by minimizing the following loss function:

$$\mathcal{L}_{total} = \lambda_1 \mathcal{L}_{KL} + \lambda_2 \mathcal{L}_{seg} + \lambda_3 \mathcal{L}_{rec} + \lambda_4 \mathcal{L}_{z-rec}, \quad (11)$$

where  $\mathcal{L}_{KL}$  is the KL Divergence measured between the sampled and the predicted style vectors,  $\mathcal{L}_{rec}$  is the image reconstruction loss,  $\mathcal{L}_{seg}$  is the anatomy segmentation loss, and  $\mathcal{L}_{z-rec}$  is the LR loss between the sampled and the re-encoded style vector.  $\lambda_1 = 0.01$ ,  $\lambda_2 = 10$ ,  $\lambda_3 = 1$ , and  $\lambda_4 = 1$  are the hyperparameters used by the authors in Chartsias et al. (2019).

### A.5 SPADE DECODER DESCRIPTION

As described in Section 4, SDNet relies on a FiLM-based decoder to combine the content and style information and reconstruct the input image. The key characteristic of FiLM is that it gradually adds style information to the content-based reconstruction process. Additionally, an alternative approach



Table 5: Comparative evaluation of SDNet (Chartsias et al., 2019) variants on the ACDC Bernard et al. (2018) dataset with 100% annotation masks, using the proposed metrics. The *Dice Score* metric is used to measure the performance in terms of semantic segmentation.

SDNet	Original Model	Design Bias		Learning Bias
		SPADE	w/o Binarization	w/o KL Divergence and Latent Regression
$DC(C, S)$ ( $\downarrow$ )	0.48	0.59	<b>0.43</b>	0.57
$DC(I, C)$ ( $\uparrow$ )	0.97	0.94	<b>0.97</b>	0.95
$DC(I, S)$ ( $\uparrow$ )	0.44	<b>0.57</b>	0.44	0.53
$IOB(I, C)$ ( $\uparrow$ )	5.66	5.63	<b>6.21</b>	3.86
$IOB(I, S)$ ( $\uparrow$ )	0.99	<b>1.02</b>	1.00	0.96
<i>Dice Score</i> ( $\uparrow$ )	0.82	0.83	0.82	0.81

for combining the content and style features is investigated, by using a SPADE decoder (Park et al., 2019) to further expose the design bias added by the decoder architecture.

A SPADE block receives the content channels and projects them onto an embedding space using two convolutional layers to produce the modulation parameters (tensors)  $\gamma$  and  $\beta$ . These parameters are then used to scale ( $\gamma$ ) and shift ( $\beta$ ) the normalized activations of the style representation. We utilize multiple SPADE blocks to fuse content and style information at different levels of granularity during decoding. A schematic of the utilized SPADE decoder in the context of SDNet is depicted in Fig. 4.

#### A.6 MEDICAL SEGMENTATION: SDNET ON ACDC (100% ANNOTATIONS)

In Section 5.2, we present the results of the SDNet model variants trained with minimal supervision, using only the 1.5% of the provided ACDC (Bernard et al., 2018) annotations. Here, we provide the results for the same experiment but using the 100% of the provided annotations. From the results reported in Table 5, it can be seen that when using strong inductive biases, such as the supervised losses in this experiment, the degree of disentanglement does not significantly affect the segmentation performance (utility).

#### A.7 DEEPFASHION DESCRIPTION AND PANET TRAINING SETUP

**Data:** We use DeepFashion (Liu et al., 2016), a large-scale dataset with over 800,000 diverse images of people in different poses and clothing, that also has annotations of body joints. We only used full-body images, specifically 32,032 images for training and 7,997 images for testing.

**Training setup:** PANet is trained in an unsupervised way with the following loss function:

$$\mathcal{L}_{total} = \lambda_1 \mathcal{L}_{rec} + \lambda_2 \mathcal{L}_{equiv}, \quad (12)$$

where  $\mathcal{L}_{rec}$  is the mean absolute error between the reconstructed and the input image.  $\mathcal{L}_{equiv}$  is an equivariance cost, that ensures that the mean and covariance of the parts coordinates don't change after some style transformation. Based on the implementation details presented in Lorenz et al. (2019), we set  $\lambda_1 = \lambda_2 = 1$ .

#### A.8 METRICS CORRELATION AND DISENTANGLEMENT-PERFORMANCE TRADE-OFF

**Metrics correlation:** As noted in Section 5.4, we argue that the proposed metrics are uncorrelated with each other. In this supplement, we aim to support the argument by measuring the correlation of the values obtained for each metric across the three applications/models. Fig. 5 depicts the Pearson correlation for the proposed disentanglement metrics. Based on the results, we confirm our intuition that the metrics are not strongly correlated. Additionally, we observe that the most correlated pair appears to be  $IOB(I, C)$  and  $DC(I, C)$ . This is supported by the fact that content representation (3D tensor) preserves more spatial information of the input than the style, where the information is encoded in a significantly lower dimensional vector. These findings support the need of using

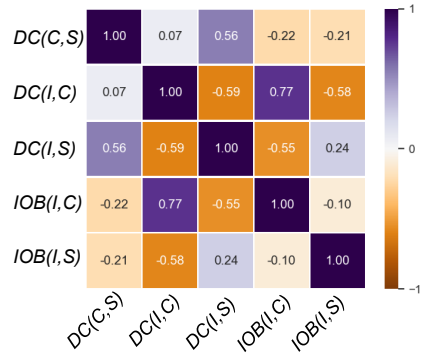


Figure 5: Pearson correlation of the proposed metrics across all applications/models visualized as heatmap. Values close to 1 and -1 indicate strong correlation.

different, but complementary, metrics to measure the informativeness and independence of the latent representation.

### A.9 QUALITATIVE EVALUATION

We visualize the content and style representations in order to reason about their interpretability. We consider the content semantic if distinct objects appear in different channels, whereas the style is semantic when images reconstructed while traversing the style manifold between two points have smooth appearance changes, and are realistic. As an extension of the samples presented and discussed in Section 5.4, here we provide visualizations for all model variants. In particular, Figs. 6 and 7 depict several channels of content, as well as style traversals for different MUNIT and SDNet model variants, respectively. However, Fig. 8 presents solely content representations, as PANet does not assume a prior distribution on the style latent vector, thus style traversals are not possible. When interpolating between two style vectors, the originally proposed MUNIT produces realistic images, and smooth appearance changes. Instead, removing the LR constraint affects the image quality. Similarly, the original SDNet presents high image quality and smooth transitions, while removing the content Binarization leads to low intensity (style) diversity.

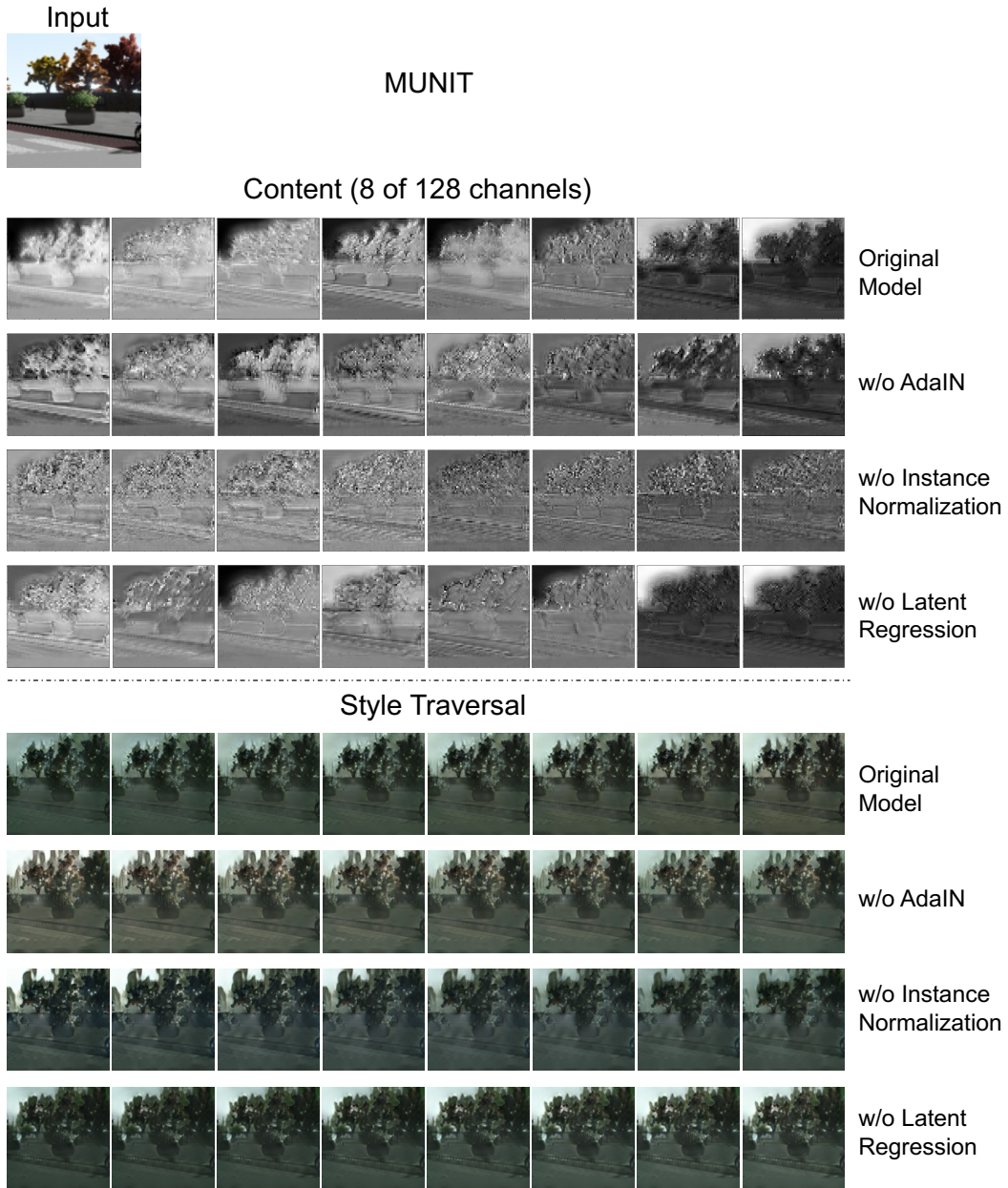


Figure 6: MUNIT: Qualitative examples to assess the interpretability of the content and style representations of the investigated model variants for different biases. For each variant, we show 8 channels of the content and 8 indicative style traversals. The input image is depicted at the top left of the figure.

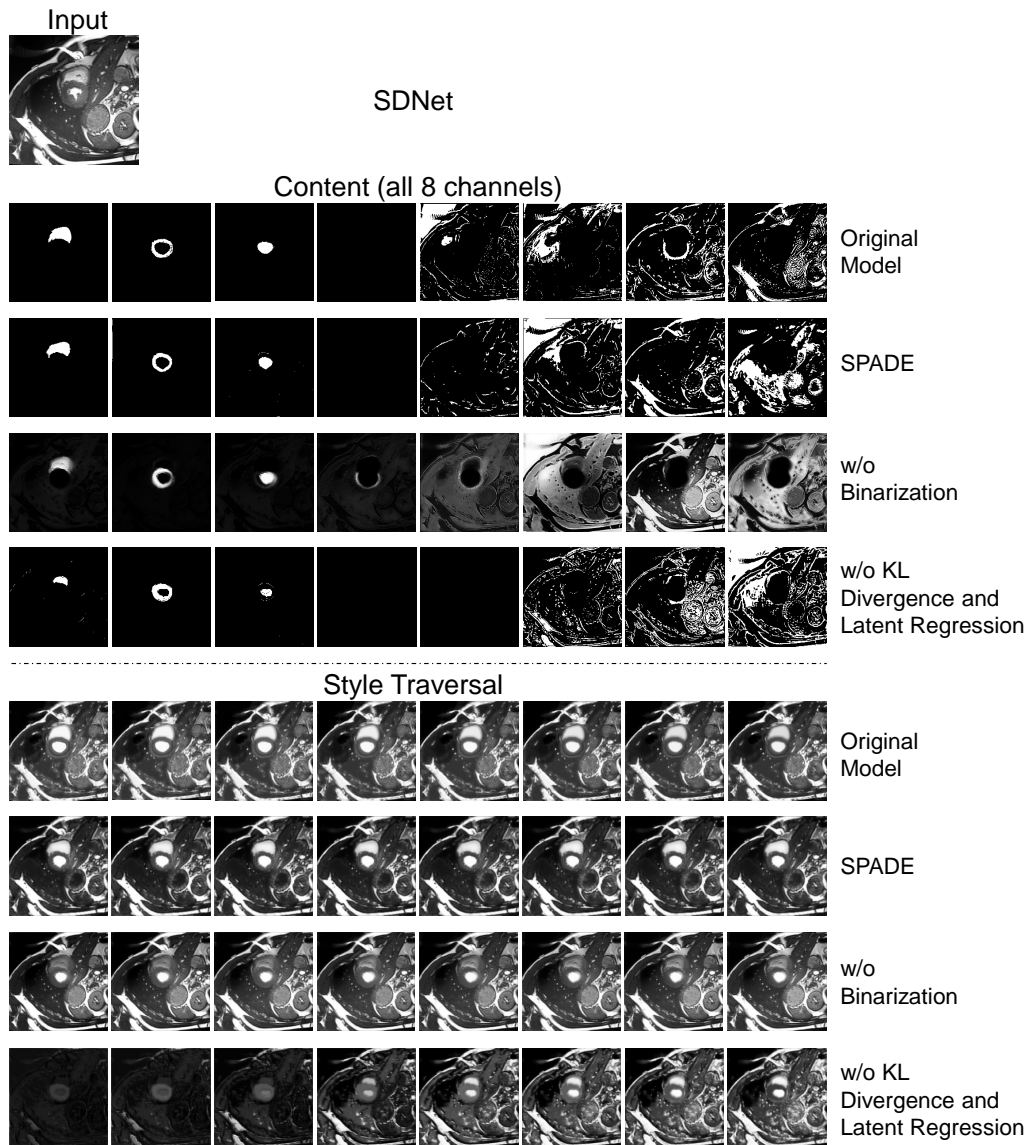


Figure 7: SDNet: Qualitative examples to assess the interpretability of the content and style representations of the investigated model variants for different biases. For each variant, we show 8 channels of the content and 8 indicative style traversals. The input image is depicted at the top left of the figure.

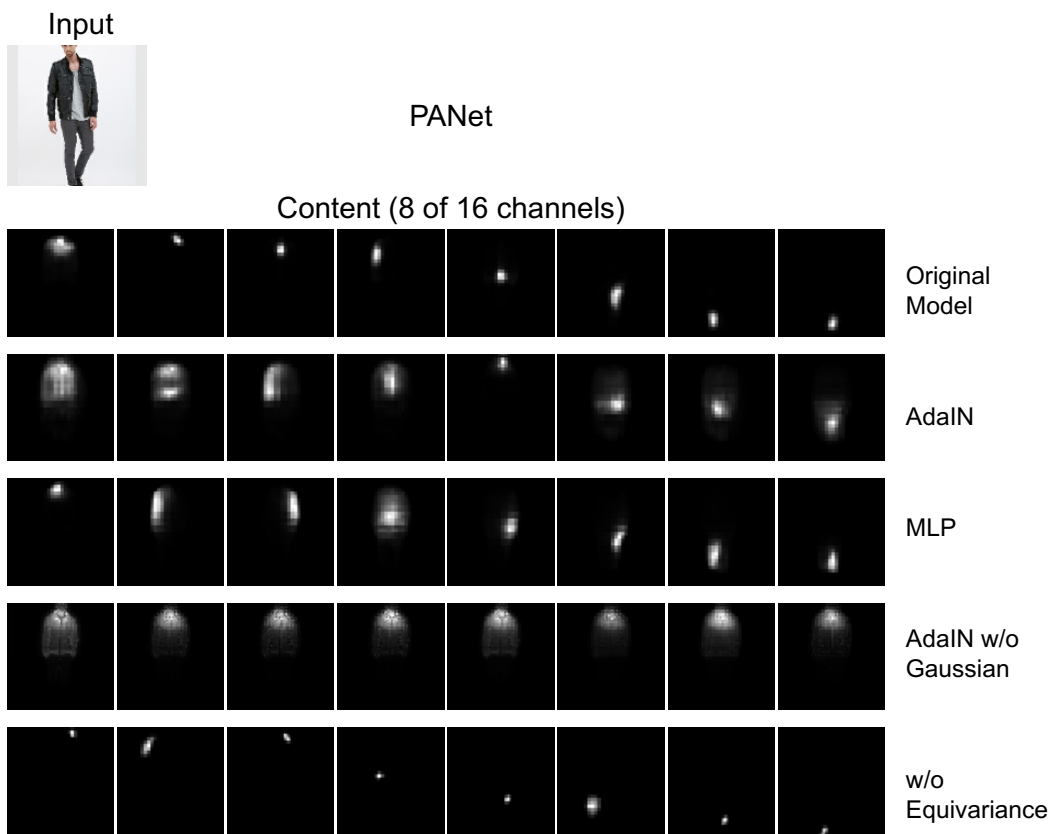


Figure 8: PANet: Qualitative examples to assess the interpretability of the content and style representations of the investigated model variants for different biases. For each variant, we show 8 channels of the content. Note that since PANet does not assume a prior distribution on the style, no style are shown. The input image is depicted at the top left of the figure.